Available online at www.sciencedirect.com

ScienceDirect

Procedia Engineering 82 (2014) 279 – 290

Procedia Engineering

www.elsevier.com/locate/procedia

23rd International Meshing Roundtable (IMR23)

Toward mixed-element meshing based on restricted Voronoi diagrams

Jeanne Pellerin[a,b,c,*], Bruno Lévy[b], Guillaume Caumon[a]

[a] GeoRessources UMR 7359, Université de Lorraine - ENSG, 54500, Vandoeuvre-lès-Nancy, France
[b] Project ALICE, INRIA Nancy Grand Est, 615 rue du jardin botanique, 54600 Villers-lès-Nancy, France
[c] Weierstrass Institute for Applied Analysis and Stochastics (WIAS), Mohrenstrasse 39, 10117, Berlin, Germany

Abstract

In this paper we propose a method to generate mixed-element meshes (tetrahedra, triangular prisms, square pyramids) for B-Rep models. The vertices, edges, facets, and cells of the final volumetric mesh are determined from the combinatorial analysis of the intersections between the model components and the Voronoi diagram of sites distributed to sample the model. Inside the volumetric regions, Delaunay tetrahedra dual of the Voronoi diagram are built. Where the intersections of the Voronoi cells with the model surfaces have a unique connected component, tetrahedra are modified to fit the input triangulated surfaces. Where these intersections are more complicated, a correspondence between the elements of the Voronoi diagram and the elements of the mixed-element mesh is used to build the final volumetric mesh. The method which was motivated by meshing challenges encountered in geological modeling is demonstrated on several 3D synthetic models of subsurface rock volumes.

Peer-review under responsibility of organizing committee of the 23rd International Meshing Roundtable (IMR23)
Keywords: restricted Delaunay triangulation ; hybrid mesh ; thin sections ; prisms ; B-Rep model ; geological modeling

1. Introduction

Representing volumetric models by their boundary surfaces (B-rep models) is particularly adapted to geological structural models that are often built from the surfaces delimiting subsurface rock volumes (Fig. 1). Generally these surfaces are triangulated [1] . In the exploration, the exploitation, and the protection of natural resources, these models are used to understand the 3D organization of subsurface rock units and to predict their behavior. For example, to assess the validity of a model or to evaluate seismic risks in an area, finite element simulations of rock mechanical deformations and of the propagation of seismic waves may be run on tetrahedral meshes of structural models [2,3]. There are several methods to mesh such multi-material models. If the input model boundaries can be subdivided, then a conforming Delaunay tetrahedralization [4] or a constrained Delaunay triangulation [5,6] can be built. When the meshes that define the boundaries between the materials cannot be modified due to some application-specific constraints, algorithms preserving them can be used [7]. In both cases, the shapes and sizes of the generated tetrahedra

* Corresponding author. Tel.: +49 30 20372-0 ; fax: +49 30 20372-303.
E-mail address: jeanne.pellerin@gocad.org

Peer-review under responsibility of organizing committee of the 23rd International Meshing Roundtable (IMR23)
doi:10.1016/j.proeng.2014.10.390

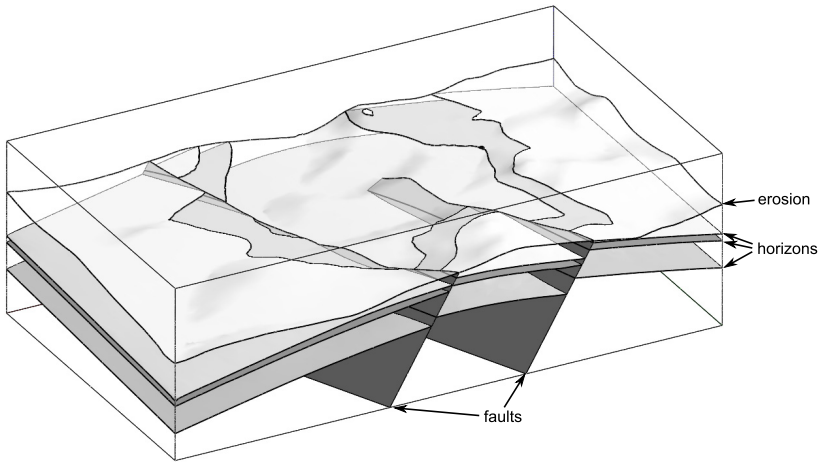

Fig. 1. Geological structural model represented by its boundary surfaces. The different stratigraphic layers are delimited by horizon surfaces, they are folded, faulted, and eroded.

depend on the model geometry and on the input surface mesh quality. The typical issue in geological modeling is that the thickness of some potentially important model components can be smaller than the desired mesh size. For example, erosion surfaces (Fig. 1) very often intersect other surfaces tangentially. To resolve this conflict between the model level of detail and the mesh size, the two main strategies are to relax the constraints on the mesh and to modify the model geometry. Our goal is to do both. We mesh the thin regions of the model with prisms to decrease the number of element used to mesh the model, and we modify the model to adapt its resolution to a limited number of elements. The resulting meshes are related to boundary layer meshes which generation generally relies on an advancing surface (or advancing facet) strategy, e.g., [8–11], or exploit the tubular geometry of blood vessels [12], or use local mesh modifications [13,14]. In the methods cited above, prisms are built either around the object, or determined by (an approximation of) the distance to the medial axis of the object (local feature size).

The method we propose to generate a mixed-element mesh (tetrahedra, prisms, pyramids) for a valid B-Rep model defined by conformal triangulated surfaces permits to control the number of cells and to modify the model. It is based on a global subdivision of the model by a Voronoi diagram, and on a local mesh building strategy. Our method does not require the user to pre-define the regions where prisms will be constructed. Our idea is to modify the restricted version of the Voronoi-Delaunay duality (Sect. 2) and propose another correspondence that considers the connected components of both the intersection of the Voronoi diagram with the regions and the intersection of the Voronoi diagram with the surfaces (Sect. 3). All cells are then built following the procedure described in Sect. 4. Some mixed-element meshes obtained with the method are shown in Sect. 5. Limitations and improvements are discussed in Sect. 6.

2. Key concepts

2.1. Voronoi and Delaunay

A Voronoi diagram is a space subdivision into several regions defined from a set of points called sites and denoted S. Each site, $p \in S$, corresponds to one Voronoi cell V_p that contains all the points of the space closer to p than to any other site q. In $\mathbb{R}^3$, when the proximity between a point x and a site p is measured by the Euclidean distance $\|x - p\|$, the Voronoi cell is defined as: $V_p = \{x \in \mathbb{R}^3 \, , \, \|x - p\| \leq \|x - q\|, \, q \in S\}$. The set of Voronoi cells constitutes the Voronoi diagram of S.

When the sites are in general position (no four co-circular sites, and no five co-spherical points), Voronoi cell facets are the points equidistant from two neighboring sites; edges are shared by three Voronoi cells, and vertices by four cells. The tetrahedron connecting the sites of these four cells is a Delaunay tetrahedron and the set of such tetrahedra

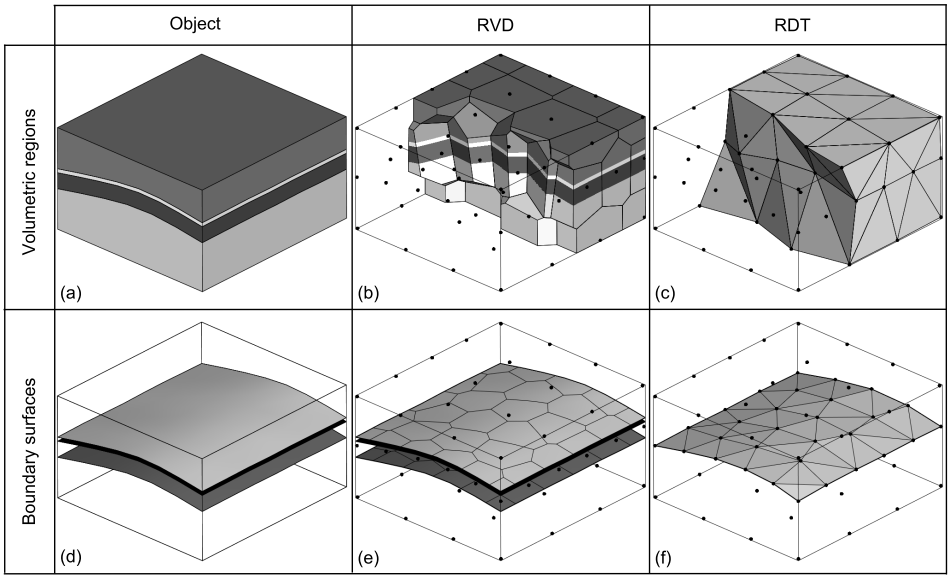

Fig. 2. Restricted Voronoi diagrams (RVD) and their dual restricted Delaunay triangulations (RDT) to a B-rep model surfaces or regions.

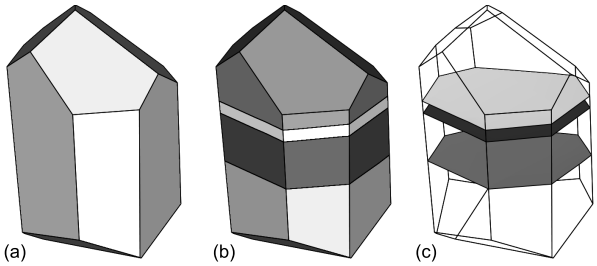

Fig. 3. (a) A 3D Voronoi cell. (b) Its restriction to the model regions has 4 connected components. (c) Its restriction to the model surfaces has 3 connected components.

constitutes the Delaunay tetrahedralization - or triangulation - of the sites. The Delaunay triangulation of the set of sites S is said dual of the Voronoi diagram of S, because to each Voronoi cell corresponds one vertex, to each Voronoi facet one edge, to each Voronoi edge one triangle, and to each Voronoi vertex one tetrahedron.

2.2. Restricted Voronoi and restricted Delaunay

The Voronoi diagram of given sites S subdivides the space in which it is defined into convex regions, therefore it subdivides any object Ω included in that space. This subdivision is called the restricted Voronoi diagram (Figs. 2b&e) which is defined as the intersection between the Voronoi diagram of S with the object Ω. In this paper, the objects of interest are the regions and the surfaces of B-Rep models (Figs. 2a&d). The intersection of a Voronoi cell, V_p, with the object Ω is called the restricted Voronoi cell of p to Ω and is defined by $V_{p\cap\Omega} = V_p \cap \Omega$ (Fig. 3). Similarly the intersection of a Voronoi edge/facet/vertex with the object is called a restricted Voronoi edge/facet/vertex.

In $\mathbb{R}^3$, the intersection of the Voronoi diagram of sites S with the regions of a 3D B-rep model gives restricted Voronoi cells/facets/edges/vertices that are either empty, or that are the complete Voronoi cell/facet/edge/vertex, or that are cut into several connected components by model boundary surfaces (Fig. 3). The intersection of the same Voronoi diagram with the model surfaces gives restricted Voronoi cells that are either empty, or that have one or several surface connected components (Fig. 3). Each restricted facet is constituted of one or several segments shared

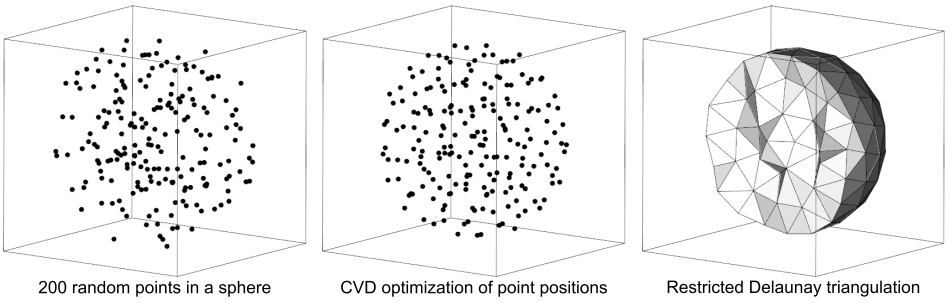

Fig. 4. Centroidal Voronoi optimization meshing principle.

by two adjacent restricted Voronoi cells. Restricted edges are the points resulting of the intersection of Voronoi edges with the surfaces.

The restricted Delaunay triangulation is defined as the dual of the restricted Voronoi diagram (Figs. 2c&f). It contains one tetrahedra for each non-empty restricted Voronoi vertex, one triangle for each non-empty restricted Voronoi facet, one edge for each non-empty restricted Voronoi facet, and one vertex for each non-empty restricted Voronoi cell. By construction, the tetrahedra, triangles, edges, and vertices of the restricted Delaunay triangulation are a subset of the Delaunay triangulation.

2.3. Centroidal Voronoi diagram

The space subdivision into Voronoi cells determined from random sites is also random. To have more control on Voronoi cell sizes and shapes, one may minimize the distances between each site and the points of its Voronoi cell. This optimization tends toward a specific Voronoi diagram: a centroidal Voronoi diagram in which each site is at the centroid of its Voronoi cell V_p. It is possible to find the locations of sites s_i in such a way that they define a Centroidal Voronoi Diagram by minimizing the following objective function [15]:

$$F_{CVD}((s_i)_{i=1...k}) = \sum_{i=1}^{k} \int_{y \in V_i} \|y - s_i\|^2 dy \tag{1}$$

where V_i is the Voronoi cell corresponding to site s_i. Similarly, the restricted Voronoi diagram of a point set S to a domain Ω is centroidal if each site p is at the centroid of its restricted Voronoi cell. The function F_{CVD} remains the same except that the integration domain is the restricted cell instead of the complete Voronoi cell.

The centroidal Voronoi diagram is one of the key elements of the variational meshing methods that consist in optimizing the positions of all final mesh vertices before building their (restricted) Delaunay triangulation (Fig. 4) [16–21]. The two features distinguishing this approach from more classical tetrahedron meshing methods is that (1) the number of vertices can be fixed and that (2) tetrahedra shape and quality are globally optimized by the objective function.

3. From a 3D restricted Delaunay triangulation to a mixed-element mesh

Our method is related to variational meshing methods, since we build a mesh from sites optimized so that their Voronoi diagram or restricted Voronoi diagram is centroidal. But, instead of building the restricted Delaunay triangulation to the model regions, we propose to take into account the connected components of the restricted Voronoi diagram to the regions and the connected components of the restricted Voronoi diagram to the model surfaces to build the final mesh. Indeed, whichever is the number of connected components of a restricted Voronoi cell/facet/edge, its dual in the restricted Delaunay triangulation will only have one connected component. That is why from four regions on the model Fig. 2b, only two remain in the restricted Delaunay triangulation Fig. 2c.

We first give two examples of the cells we propose to build. When close to surface boundaries, restricted Voronoi cells to the regions can intersect one surface (Fig. 5a). In the classical Voronoi-Delaunay relationship, the dual of a

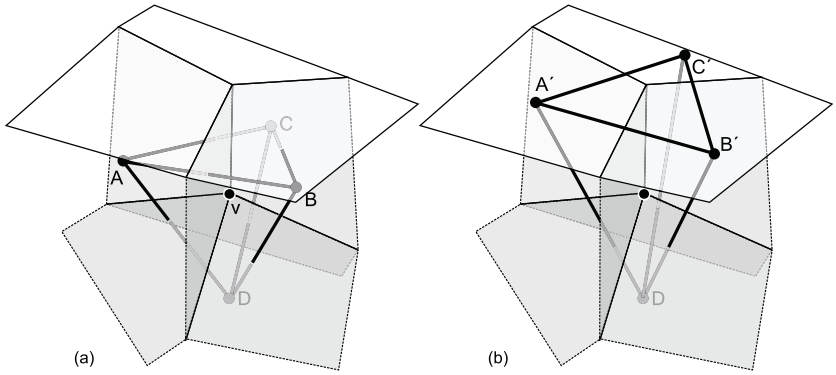

Fig. 5. Delaunay tetrahedron modification near one surface.

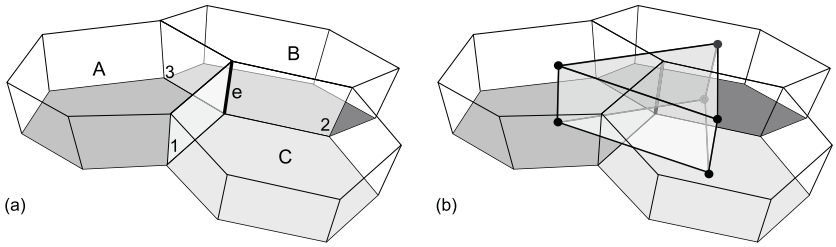

Fig. 6. Prism built to mesh a thin section, it corresponds to the restricted Voronoi edge to this thin section e.

Table 1. Relationship between mixed-element mesh elements and restricted Voronoi diagrams elements. Each final mesh element corresponds to one element of the restricted Voronoi diagram to the model regions according to the number of connected components (cc) of this restricted Voronoi diagram element to the model surfaces.

Mesh element		Configuration		Example
		Volume RVD	Adj. surfaces	
1	**Vertex**	Cell cc	<2	cells A,B,C,D, Fig. 5
2			>1	cells A,B,C Fig. 6
1	**Edge**	Cell cc	>1	cells A,B,C Fig. 6
1		Facet cc	<2	all facets Fig. 5
2			>1	facets 1,2,3, Fig. 6
1	**Facet**	Facet cc	>1	facets 1,2,3, Fig. 6
1		Edge cc	<2	all 6 facets, Fig. 5
2			>1	edge e, Fig. 6
1	**Cell**	Edge cc	>1	edge e, Fig. 6
1		Vertex	0	vertex v, Fig. 5

point shared by such cells is a tetrahedron linking the four sites. We propose to modify the tetrahedron vertices and instead of the sites, take the centroids of the adjacent restricted Voronoi diagram to the surfaces (Fig. 5b). In thin sections of the model, restricted Voronoi cells to regions can intersect several times the model surfaces (Fig. 3). The connected components sandwiched between two surfaces may then not contain any Voronoi vertex (for example cells A, B, and C on Fig. 6 share only a restricted Voronoi edge e). By putting one vertex at the centroid of each restricted Voronoi cell to the surfaces, a prism corresponding to e can be built (Fig. 6b). To formalize the building of these cells, we propose to put in correspondence the cells, facets, edges, and vertices of the Voronoi diagram cut into several parts by the model surfaces (Fig. 3) with the cells, facets, edges, and vertices of a mixed element mesh (Tab. 1). One or two vertices of the final mesh are associated to each volumetric restricted Voronoi cell depending on the number of adjacent surface connected components.

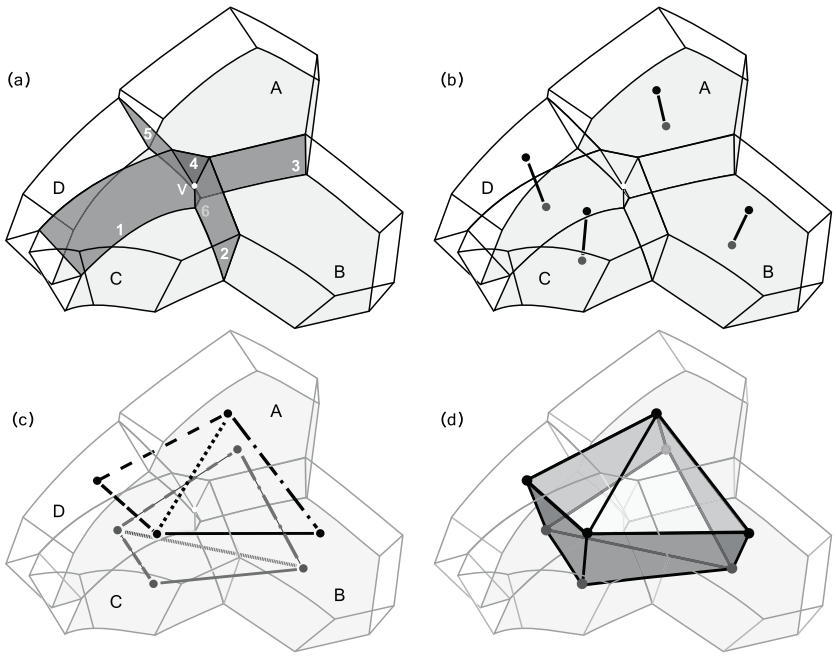

Fig. 7. Cell building. (a) Restricted Voronoi vertex v to a thin section is shared by four restricted Voronoi cells (A, B, C, D), 6 facets, and 4 edges. (b) To each restricted cell correspond two vertices and one edge. (c) To each facet correspond one (facets 4 and 6) or two edges (facets 1, 2, 3 and 5). (d) Final cell has eight vertices, 4 triangle facets, and 4 quad facets.

4. Cell building algorithm

To build all the cells automatically whatever the configuration of their intersections with the model regions and surfaces, we propose an algorithm that consists of the following steps. First the cells to build are determined by identifying their corresponding restricted Voronoi edges and vertices. They are then built one by one by adding successively their vertices, edges, and facets. The procedure is illustrated for a restricted Voronoi vertex to a thin section sandwiched between two boundary surfaces (Fig. 7a).

4.1. Vertices

For each of the four (resp. three) volumetric restricted Voronoi cell containing the restricted Voronoi vertex (resp. edge), there is one or two points to add to the cell. If the restricted cell does not intersect model surfaces, that point is the site of the cell. If it does, the centroids of these intersections (adjacent connected component of the restricted cell to the surfaces) are taken for the points. When there are more than two intersections, some points are merged at their centroid so that there is maximum two points per restricted cell. For example, on Fig. 7a, each restricted cell that contains vertex v is adjacent to two surface connected components and corresponds to two points (Fig. 7b).

4.2. Edges

There are two types of edges to add: those linking the points corresponding to the same Voronoi cell (Fig. 7b), and those corresponding to Voronoi facets containing v (Fig. 7c). Each of the facets 1, 2, 3, 5 corresponds to two edges; the small triangular facets 4 and 6 intersect once the model surfaces and correspond to a unique edge in the cell to build.

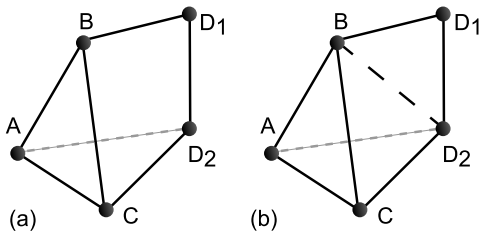

Fig. 8. Invalid cells with 5 vertices. (a) Vertices D_1 and D_2 correspond to the same Voronoi cell. Facets ABD_1D_2 and BCD_1D_2 share three vertices. (b) Cutting these facets with BD_2 results in a tetrahedron plus a triangular facet.

4.3. Facets

The first facets to add are those corresponding to the four restricted edges containing v. They are built from the edges corresponding to the restricted facets containing the restricted edge. In our example, they are all triangles (Fig. 7d), but in the general case they could be polygons with up to six vertices. The other facets to add correspond to the restricted Voronoi facets containing v that are adjacent to at least two surface connected components. The four gray quad facets on Fig. 7d correspond to restricted facets 1, 2, 3 and 5 on Fig. 7a.

4.4. Finalizing the current cell

Once all vertices, edges, and facets have been added to the cell, the cell type is determined from the number of these elements. Theoretically, a mixed-element cell created with the above algorithm may have four to eight vertices, six to sixteen edges, four to ten facets, each facet having up to six vertices. In practice, most of the cells are tetrahedra, prisms, or pyramids. The other cells are processed as follows.

They are first sorted into three categories: (1) the cells to subdivide (cells with 7 or 8 vertices defining a valid volume, Fig. 7d), (2) invalid cells (in which at least one edge is a diagonal of a facet, or in which two quad facets share more than two vertices, like 5-point cells which are relatively abundant, see Fig. 8a) and (3) the cells that belong to none of the above categories.

Cells to subdivide are subdivided by adding a vertex at their centroid and building pyramids and tetrahedra with their facets. To compute tetrahedra, pyramids, and prisms from invalid cells, a two step procedure is implemented. First, all facets that are inconsistent with some edges are split along these edges. Then the validity of cell facets must be ensured. Facets with more than four vertices are triangulated and quad facets that share three vertices with another facet are split (Fig. 8b). This processing permits to reduce the number of invalid cells, but is not sufficient to obtain a final valid mesh in all cases.

5. Results

We experimented our mixed-element meshing method with both geological and non-geological models. Computational time (between several seconds and several minutes on a laptop with a 8 cores 1.73GHz Inter Core i7 processor and 8 GB of RAM) depends on the number of sites, on the input model number of triangles, and on the number of invalid cells to process. Different model sampling strategies were used, initial random points being either optimized to have a centroidal restricted Voronoi diagram to the model regions, or to have a centroidal restricted Voronoi diagram to the model surfaces, or both. As suggested by [24] we use a Newton-like method to minimize F_{CVD}. The computation of the restricted Voronoi diagrams to the regions and to the surfaces are done using the methods implemented by [21] and [25].

The meshes obtained for models in which layer thicknesses do not vary significantly and that have smooth boundaries, such as three nested spheres, Fig. 9, reproduce boundary layer meshes. It is not only the number of sites sampling the spheres that determines which layers are thin and meshed with prisms, but also the positions of these sites and the way they were optimized (Fig. 10). The heptoroid model that has a complex topology (Fig. 11) is meshed

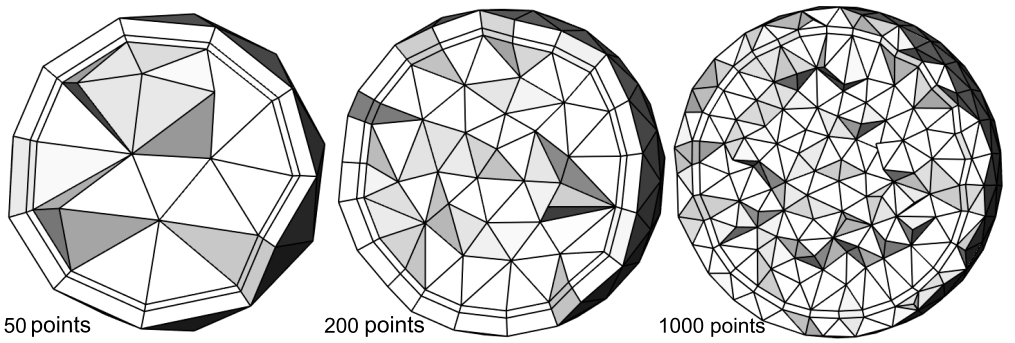

Fig. 9. Three nested spheres meshed at three resolutions. With 50 and 200 points the two layers are meshed with prisms, while with 1000 points the external layer is meshed with tetrahedra.

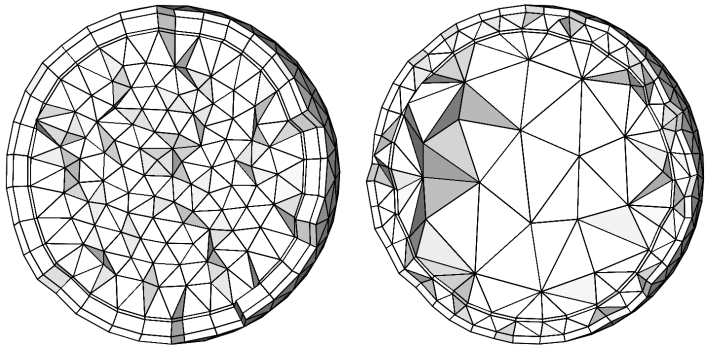

Fig. 10. Two meshes of 4 nested spheres computed from 1,000 points. Left: the points were optimized to get a centroidal Voronoi diagram inside the smallest sphere. The three external layers are meshed by prisms. Right: 950 points were optimized to get a centroidal restricted Voronoi diagram to the 4 spheres while 50 points sample the interior of the smallest sphere. The thickest layer is meshed with tetrahedra, and the other two with prisms.

(11 seconds) from only 1010 sites. However the model is pinched near its extremities because only one site samples both creases and each restricted Voronoi cell to the surface has one connected component.

Results for synthetic geological models are promising (Figs. 12 and 13). The thinnest layer of the simple fold model on the top of Fig. 12 is completely meshed with prisms. In the second model, built from the first by adding two faults that cut and displace the layers (one of them not cutting through the model), the same thin layer is also meshed with prisms. The discontinuities induced by the faults are respected in the mesh. However, like on Fig. 11, the layer is pinched near the faults and near the model box, an approximation that may be undesirable. The third model is built from the second by adding an erosion surface, below which remaining layers can be very thin and which can intersect other surfaces tangentially. In that case the ability to not fully respect the input model is crucial to limit the number of elements in the final mesh. The mesh obtained for another type of model characterized by very thin layers, major layer thickness variations, and small angle contacts between layers due to onlapping geometries is also very promising (Fig. 13). An adequate sampling is the key for our method to succeed. Here 5,000 sites were optimized so that their restricted Voronoi diagram to the model surfaces is centroidal, 500 points and 750 points sampling (volumetric centroidal Voronoi diagram optimization) the top and the bottom regions were added to these.

6. Discussion

We proposed a method to generate a mixed-element mesh (tetrahedra, prisms, pyramids) from the intersection of the Voronoi diagram of given points and a B-Rep model. The Voronoi diagram that we use realizes a global subdivision of the model, permitting to analyze the model at the mesh building step, while globally controlling its resolution. The

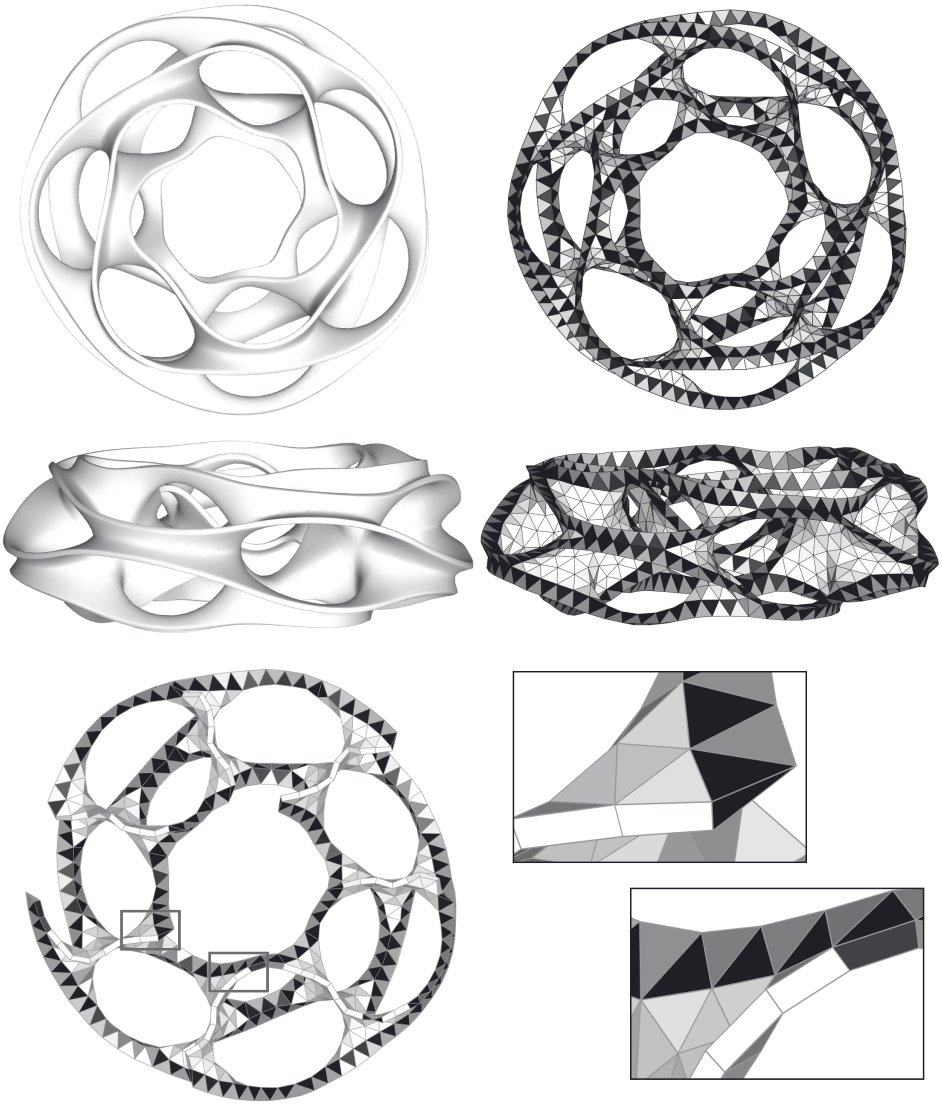

Fig. 11. Mixed element mesh inside a smooth heptoroid surface, 516 tetrahedra (gray), 665 prisms (white), and 507 pyramids (black).

type of the elements built depends on the local thickness of the region considered and on the positions of the points sampling the model. However, the choice of the number of points is currently left to the user's intuitiveness. Additional work is needed to link this number with the input model geometry, the desired output model representation, and the desired mesh edge length. No preliminary identification of the thin sections, that are meshed with prisms, is required. Note that no prism will be generated in non-thin regions, this could be achieved by adding virtual offset surfaces inside the regions. The final mesh does not depend on the input triangulation of the model surfaces (the only requirement is that their meshes are conformal). Indeed the surfaces are remeshed when the mixed-element mesh is built. The related surface remeshing method has been described by [26].

The main limitation of our approach is that some final cells are non-valid, in the sense that they do not define a valid volume, and may intersect neighboring cells. Like for octree meshing methods, the difficulty is that all possible configurations for the intersections between subdivision cells and the model do occur. Having a control on these intersections is one of the reasons why the points are optimized so that their (restricted) Voronoi diagram is centroidal,

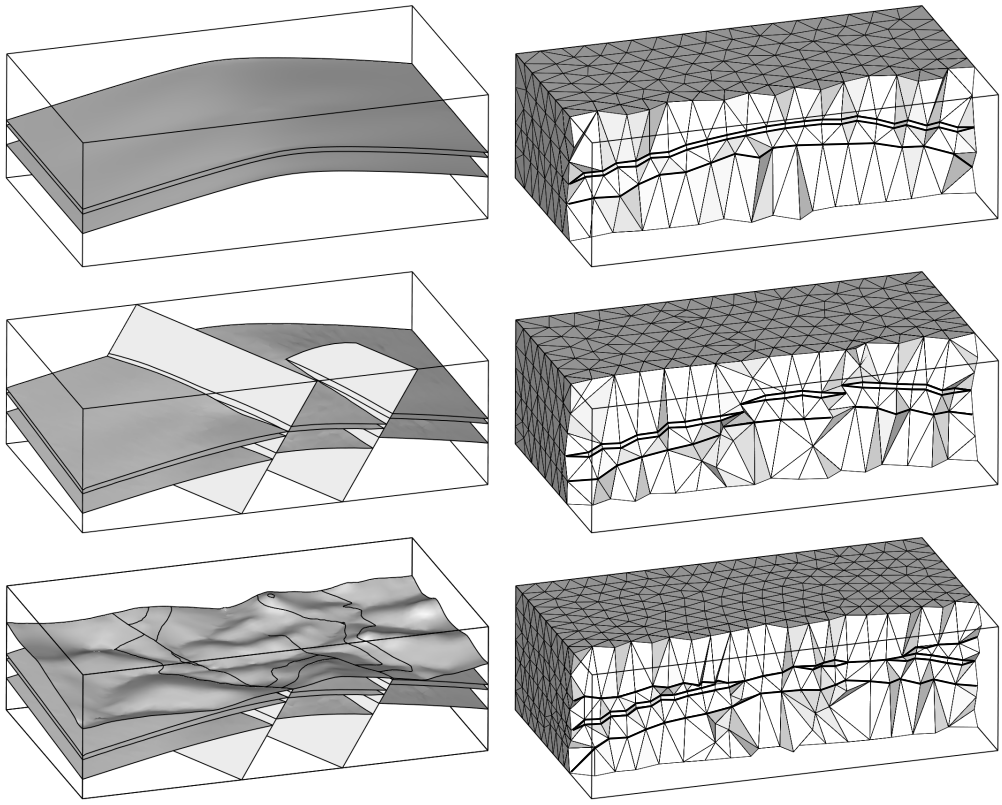

Fig. 12. Hybrid meshes for 3 synthetic geological models [22]. Region boundaries are highlighted.

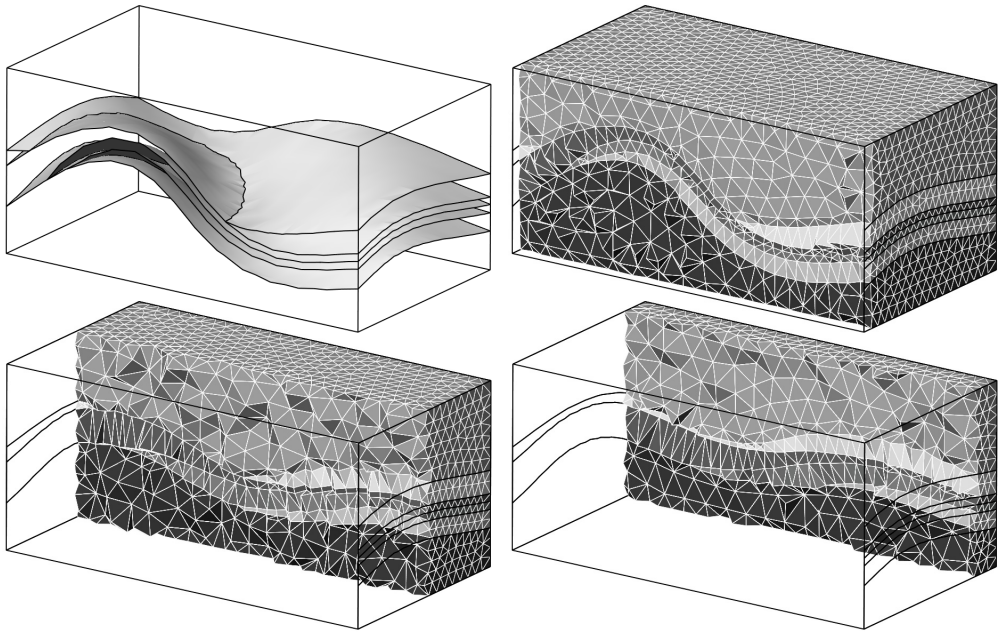

Fig. 13. Solid slices in a hybrid mesh of a synthetic model [23]. Gray shades correspond to the 6 model regions.

and why many (re)meshing methods based on such an optimization refine the model sampling so that cell intersections with the model have a unique connected component (and verify the topological ball property [27]). Because with our method prisms are built when restricted Voronoi cells have several connected components, we cannot use this last condition and we need to develop one adapted to our mesh building method to improve site placement and determine the adequate number of points.

However, we do think that the fact that the algorithm fails for some cells is a show stopper, because, before a fully satisfactory solution is found, whenever the algorithm does not successfully generate a polyhedral cell, it is still possible to generate tetrahedra in cavities corresponding to the cells where the algorithm failed. The second possibility is to completely change the cell building strategy, and instead of building a mesh from scratch, progressively modify the Delaunay triangulation of the sites by local valid operations (vertex displacement, vertex/edge/facet duplication) that would permit to obtain the desired conformal mixed element mesh. Indeed, the invalid cells we obtain correspond to modifications of the Delaunay triangulation that break the mesh validity. For instance, as shown on Fig. 8, whenever a restricted Voronoi cell intersects the set of surfaces twice, it may generate a cell with 5 vertices, due to the considered vertex that will be duplicated. In addition, note that when duplicating a vertex and moving the two instances at different locations (i.e., at the centroid of the restricted Voronoi cell connected components), special care is needed to avoid generating inverted elements (i.e. with negative orientation/Jacobian).

Acknowledgements

This works has been performed in the frame of the Gocad research project (http://www.gocad.org/w4/) and of the “Investissements d’avenir” Labex RESSOURCES21 (ANR-10-LABX-21). We thank the industry and academic members of the Gocad Research Consortium for supporting this research.

References

[1] G. Caumon, P. Collon-Drouaillet, C. Le Carlier de Veslud, J. Sausse, S. Viseur, Surface-based 3d modeling of geological structures, Mathematical Geosciences 41 (2009) 927–945.
[2] P. Durand-Riard, L. Salles, M. Ford, G. Caumon, J. Pellerin, Understanding the evolution of syn-depositional folds: Coupling decompaction and 3d sequential restoration, Marine and Petroleum Geology 28 (2011) 1530–1539.
[3] P. G. Lelievre, C. G. Farquharson, C. A. Hurich, Joint inversion of seismic traveltimes and gravity data on unstructured grids with application to mineral exploration, Geophysics 77 (2012) K1–K15.
[4] D. Cohen-Steiner, E. Colin de Verdiere, M. Yvinec, Conforming delaunay triangulations in 3d, Computational Geometry 28 (2004) 217 – 233. Special Issue on the 18th Annual Symposium on Computational Geometry - SoCG2002.
[5] J. R. Shewchuk, Constrained delaunay tetrahedralizations and provably good boundary recovery., in: Proc. 11th International Meshing Roundtable, 2002, p. 193–204.
[6] H. Si, K. Gärtner, 3d boundary recovery by constrained delaunay tetrahedralization, International Journal for Numerical Methods in Engineering 85 (2011) 1341–1364.
[7] P. L. George, H. Borouchaki, E. Saltel, Ultimate robustness in meshing an arbitrary polyhedron, International Journal for Numerical Methods in Engineering 58 (2003) 1061–1089.
[8] R. V. Garimella, M. S. Shephard, Boundary layer mesh generation for viscous flow simulations, International Journal for Numerical Methods in Engineering 49 (2000) 193–218.
[9] O. Sahni, K. E. Jansen, M. S. Shephard, C. A. Taylor, M. W. Beall, Adaptive boundary layer meshing for viscous flow simulations, Engineering with Computers 24 (2008) 267–285.
[10] V. Dyedov, D. R. Einstein, X. Jiao, A. P. Kuprat, J. P. Carson, F. del Pin, Variational generation of prismatic boundary-layer meshes for biomedical computing, International Journal for Numerical Methods in Engineering 79 (2009) 907–945. WOS:000269362300001.
[11] Y. Ito, A. M. Shih, B. K. Soni, Hybrid mesh generation with embedded surfaces using a multiple marching direction approach, International Journal for Numerical Methods in Fluids 67 (2011) 1–7.
[12] E. Marchandise, C. Geuzaine, J. Remacle, Cardiovascular and lung mesh generation based on centerlines, International Journal for Numerical Methods in Biomedical Engineering 29 (2013) 665–682.
[13] A. Loseille, R. Löhner, Robust boundary layer mesh generation, in: Proceedings of the 21st International Meshing Roundtable, Springer, 2013, p. 493–511.
[14] X.-J. Luo, M. S. Shephard, L.-Z. Yin, R. M. O’Bara, R. Nastasi, M. W. Beall, Construction of near optimal meshes for 3d curved domains with thin sections and singularities for p-version method, Engineering with Computers 26 (2010) 215–229.
[15] Q. Du, V. Faber, M. Gunzburger, Centroidal voronoi tesselations: Applications and algorithms, SIAM Review 41 (1999) 637–676.
[16] Q. Du, D. Wang, Tetrahedral mesh generation and optimization based on centroidal voronoi tessellations, International Journal for Numerical Methods in Engineering 56 (2003) 1355–1373.

[17] P. Alliez, D. Cohen-Steiner, M. Yvinec, M. Desbrun, Variational tetrahedral meshing, ACM Transactions on Graphics 24 (2005) 617–625.
[18] J. Tournois, C. Wormser, P. Alliez, M. Desbrun, Interleaving delaunay refinement and optimization for practical isotropic tetrahedron mesh generation, ACM Transactions on Graphics 28 (2009) 1.
[19] J. Tournois, Optimisation de maillages, Thèse, Université Nice Sophia Antipolis, 2009.
[20] J. Dardenne, S. Valette, N. Siauve, N. Burais, R. Prost, Variational tetrahedral mesh generation from discrete volume data, The Visual Computer 25 (2009) 401–410.
[21] B. Lévy, Y. Liu, L_p Centroidal Voronoi tessellation and its applications, ACM Transactions on Graphics 29 (2010) 1.
[22] J. Pellerin, Prise en compte de la complexité géométrique des modèles structuraux dans des méthodes de maillage fondées sur le diagramme de Voronoï, Ph.D. dissertation, Université de Lorraine, 2014.
[23] G. Laurent, Prise en compte de l'histoire géologique des structures dans la création de modèles numériques 3D compatibles, Ph.D. dissertation, Université de Lorraine, 2013.
[24] Y. Liu, W. Wang, B. Lévy, F. Sun, D.-M. Yan, On centroidal voronoi tessellation - energy smoothness and fast computation., in: ACM Transactions Graphics, 2009, pp. 1–17. 30p.
[25] D.-M. Yan, B. Lévy, Y. Liu, F. Sun, W. Wang, Isotropic remeshing with fast and exact computation of restricted voronoi diagram, ACM/EG Symposium on Geometry Processing / Computer Graphics Forum 28 (2009) 1145–1454.
[26] J. Pellerin, B. Lévy, G. Caumon, A. Botella, Automatic surface remeshing of 3d structural models at specified resolution: A method based on voronoi diagrams, Computers & Geosciences 62 (2014) 103 – 116.
[27] H. Edelsbrunner, N. Shah, Triangulating topological spaces, International Journal of Computational Geometry & Applications 7 (1997) 365–378.